Causal Scissor: root cause discovery via the measure of edge cuts in graphs

Jingi Ju[*], **Mincheol Shin**[*], **Minwoo Kim, Giwoong Lee, Jiseung Ahn, Jeongyeol Choe**[†]
IOPS
{jingi.ju,shinmc9,kimminu09,gwlee0524,jsahn,jychoe}@i-ops.co.kr

Abstract

We propose a novel causal discovery, Causal Scissor, which captures the causal flows in graphs through the lens of the mechanism of edges to elucidate root causes. Causal discovery from observed data provides interpretable relationships between the variables, with latent causal structures playing a pivotal role in explaining practical downstream tasks such as finance, industry, climate, society, and genomics. Recently generative models are studied for causal representation learning toward disentanglement and identifiability on latent causal structures to uncover the hidden information like causal discovery via perturbation conditions on biological cells. However the interdependency of causal flows in conjunction with intervention is less explored. This paper presents the identifiability of root causes through Causal Edge Cut (CEC) from causal graphs. The key to identifying root causes lies in the Barycenter Subtrees (BS) via permutations and Cholesky decomposition. To measure the causal edge cut, we utilize BS and Gromov-Wasserstein distance as a support to ensure high expressiveness on local Ollivier-Ricci curvature. Causal Scissor, the causal walk or flow in a strongly perturbed subtree with its knock-on edges and a root cause, clarifies how the causal structures by perturbation have knock-on effect due to the root cause on biological datasets such as flow cytometry and fMRI9.

1 Introduction

The status quo of scientific discovery comes with causal discovery nourished by deep neural networks. The front line of causality is the causal representation learning which uncovers the causal structures with observed data to disentangle the underlying factors to solve downstream tasks in the perspective of intervention, interaction, and treatment outcomes [20, 1, 37, 17]. In genomics, it is foremost to figure out the biological principles of interventional effects or find the root causes and treatment targets influenced by perturbation. For example, Perturb-seq [7] for bone marrow-derived dendritic cells, cell line K562, and cell line RPE1 would be considered valuable in the causal discovery of cellular biology because of their diverse interventions, data points, and features [3, 2, 29].

The causal flow of latent information matters to explain the intrinsic mechanisms in causal graphs. As a way of causal flow, curvature-based optimal transport is suggested that observed data is mapped onto geometric space to disentangle the underlying variables against such as the bottleneck problem via Ollivier-Ricci curvature (ORC) or Forman-Ricci curvature (FRC) [35, 9, 11, 10].

Our simple but interesting and meaningful finding on causal structures related to anomalies or intervention is that contextual anomalies can be detected through message passing even when it only leverages 1-hop structural information between the perturbed and non-perturbed causal graphs. Such

[*]Equal contribution
[†]corresponding author

Accepted to the NeurIPS 2025 Workshop on CauScien: Uncovering Causality in Science.

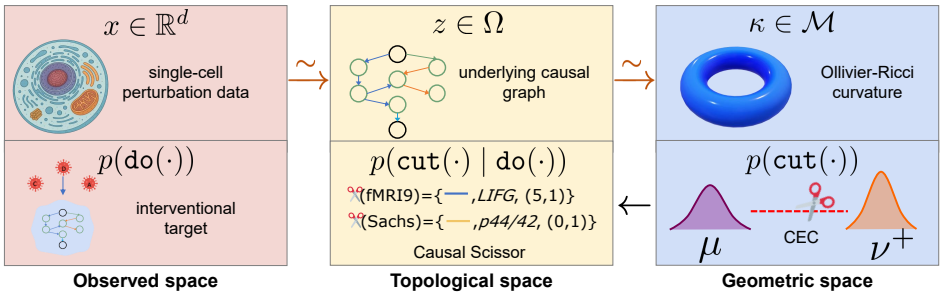

Figure 1: Embracing three spaces on biological data in the center of causal graphs, Causal Scissor discovers the strongly disturbed subtrees containing root causes and knock-on edges in graphs as shown in the lower part of topological space. $\texttt{do}(\cdot)$, $\texttt{cut}(\cdot)$ stand for perturbation and causal edge cut respectively.

signatures show changes in the pattern of edges being removed around particular nodes or sequences. Based on the point, we speculate if the root-cause nodes do not affect other child nodes any more, the edges between root causes and child nodes may be strongly cut due to the perturbation in that the underlying variables have different topological and geometric characteristics on causal graphs.

To this end, we formalize an expressive causal flow to measure root causes and strongly affected edges that quantifying edge cuts in causal graphs via Wasserstein metrics serves us the interpretability among causal variables. Causal Scissor is the framework of causal discovery and causal edge cut, the measure of Causal Scissor, calculates the conditional probability of causally removed edges for a given perturbation with Barycenter subtrees and Gromov-Wasserstein supports.

Our main questions and contributions to bridge perturbation and causal structures in science are as follows:

- *What are the causal structures under perturbation on real-world scientific data?* The structure of Causal Scissor, a causal walk of strongly perturbed subtrees, is relatively any of negatively curved simplex. We discover that Causal Scissor with the knock-on edges and root causes resides in the local minima of Fréchet energy under perturbation as edge cuts by perturbation break down the subtree-wise messages known as knock-on effect. Root causes take the subtrees with the top barycenters based on Gromov-Wasserstein support.
- *How to measure the mechanism of causal structures?* Simultaneously capturing the local and global information by using Ollivier-Ricci curvature and Gromov-Wasserstein distance, the perturbed underlying causal structure is measured. To map observed data onto topological and geometric spaces, we use a causal discovery model to infer causal graphs and calculate the perturbed causal structures via the probability of Causal Edge Cut.

2 Causal Scissor

To tackle the two questions in Introduction, our primary interest proceeds from the assumption that perturbations can change the number of connected edges on a causal graph with a certain pattern. Given biological data, we train a Bayesian optimization model (e.g. DrBO) in DAG-structured causal graphs. Starting from the root node, depth-first search (DFS) [32] to partition the graph into subtrees, one for each child of the root, is performed. Based on the subtree-wise degree of perturbation in the center of root causes, we propose Causal Scissor explaining how the perturbation works toward particular edges on manifold space. The main operation of Causal Scissor is that, in a causal graph $\mathcal{G}$, the adjacency matrix A is mapped onto manifold in curvature metrics, after which strongly perturbed subtrees are detected to jointly provide root causes and knock-on edges. To measure the Causal Scissor on geometric space, we combine the Wasserstein-1 distance W_1 in Ollivier–Ricci curvature (ORC), the Gromov–Wasserstein (GW) distance, and the Wasserstein-2 barycenter W_2^2. By the mapping functions, we obtain Causal Edge Cut (CEC) measures per subtree in the causal graph, from which Causal Scissor, consisting of the top-perturbed subtree, root causes, and knock-on edges, is determined.

Causal Edge Cut (CEC) To measure informative causal flow, curvature-based methods are proposed which are robust to the oversquashing problem in graphs. From an opposite viewpoint of [12] that curvature-based rewiring mitigates the oversquashing effect based on discrete Ricci curvature, we take curvature-based cutting that helps approach the knock-on effect based on Ollivier-Ricci curvature. We assume that perturbations change the edge states of neighboring nodes with four types described in Appendix, altering the optimal transport and the resulting curvature. Accordingly, we compute the curvature difference between the non-perturbed and perturbed conditions $\Delta\kappa = \kappa_{non} - \kappa_{do}$, where κ_{non} and κ_{do} denote the curvature under the non-perturbation and perturbation respectively. Edges with a large negative $\Delta\kappa$ are considered as strongly affected edges, i.e. knock-on edges.

The Gromov–Wasserstein distance between two metric–measure spaces is defined via a coupling that minimizes the distortion between their internal distance structures. Given two metric–measure spaces (X, d_X, μ_X) and (Y, d_Y, μ_Y), the (p, q)-Gromov-Wasserstein distance between X and Y is [21]

$$GW_p(\mu_X, \mu_Y) := \inf_{\pi \in \Pi(\mu_X, \mu_Y)} \left(\int \int_{X \times Y} \Delta_q^p d\pi \otimes \pi \right)^{\frac{1}{p}}, \tag{1}$$

where $\Pi(\mu_X, \mu_Y)$ denotes the set of couplings between μ_X and μ_Y. As the GW distance aligns internal distance structures rather than absolute coordinates or features, it is suited to quantifying structural discrepancies when non-perturbed and perturbed causal graphs are considered as manifold curvatures. Depending on the GW distance computed for each perturbation, we set the mean as a threshold and select perturbations whose distances exceed this threshold as exhibiting the substantial change of the causal structure. The criteria via GW distance is regarded as the support for each latent variable, and the set of selected perturbations is subsequently used as a first-stage filter for identifying knock-on edges.

CEC integrates ORC, GW, and root causes to estimate the probability of cut edges, especially knock-on edges, $p(\texttt{cut}(\cdot) \mid \texttt{do}(\cdot))$, thus capturing how much the perturbation flows along the edges. First, we measure the global structural distortion induced by perturbation via the GW distance; using the mean GW distance over perturbations as a threshold, we select only perturbations above this threshold. Subsequently, for each selected perturbation, we measure the non-perturbed and perturbed ORCs to identify the knock-on edges. Finally, over all selected perturbations, we aggregate and normalize the occurrence counts of knock-on edges within subtrees containing a root cause to compute $p(\texttt{cut}(\cdot) \mid \texttt{do}(\cdot))$; the higher CEC probabilities indicate the more strongly influenced edges by the perturbation.

Top-perturbed Subtree To obtain a more fine-grained causal flow for perturbation effects, we compute the subtree Wasserstein-2 barycenter. Let $\Delta_p = \left\{\lambda = (\lambda_1, ..., \lambda_p) \in \mathbb{R}^d \,:\, \lambda_i \geq 0,\, \sum_{i=1}^p \lambda_i = 1\right\}$. For marginals $\{\mu_i\}_{i=1}^p \subset \mathcal{T}, ac(\mathbb{R}^d)$ and weights $\lambda \in \Delta_p$, the subtree Wasserstein-2 barycenter is

$$\overline{\nu}_\lambda = \underset{\mu \in \mathcal{T}, ac(\mathbb{R}^d)}{\operatorname{argmin}} \frac{1}{2} \sum_{i=1}^{T} \lambda_i W_2^2(\nu, \mu_i), \tag{2}$$

where $\mathcal{T}$ is the subtree set of edge marginals. Since we let an equal λ_i, barycenter is denoted by $\overline{\nu}$. Barycenter is interpreted as the mean of a set of empirical probability under optimal transport in the space of measures, which is also known as Wasserstein barycenter and is the measure that minimizes the sum of its Wasserstein distance to each element in the set. W_2 Wasserstein barycenter is also interpreted as minimizing the Fréchet energy [27]. For a subtree-barycenter representation, we reflect it into negative Fréchet energy, $-E_F(\nu)$. In other words, the negative Fréchet energy is minimized by computing, for each subtree barycenter, its ground subtree barycenter containing Causal Scissor.

To infer root causes in a causal graph, we employ a combination of permutations and the Cholesky decomposition proposed in [19]. A root cause is the node or the set of graph features that responds to a perturbation by producing a significant change in the post-graph distribution. The subtrees of root causes contain a greater number of knock-on edges than other subtrees so that demonstrate higher barycenter and lower Fréchet energy. Thus, we regard the root causes as the local minima of the Fréchet energy evaluated with respect to the Wasserstein-2 barycenter, as illustrated in Figure 3 schematically exhibiting an energy well. As shown in Figure 2 (a), the barycenter subtrees containing relatively more root causes are observed to be in the highest as the top-perturbed subtrees.

Causal Scissor is a tuple-like set of three elements on a given dataset, ✂(data)= $\{BS, RC, KOE\}$, where BS is the top-perturbed subtree selected on the basis of the barycenter and the root causes. RC represents the root cause caused by the perturbation that maximizes the GW distance before versus after perturbation, while KOE means the knock-on edges ranked highest by CEC probability for that perturbation. In summary, Causal Scissor combines ORC, GW, the barycenter, and root causes to jointly determine the most perturbation-sensitive subtree along with its internal root cause and knock-on edges. As an example of our causal discovery, the Causal Scissor of fMRI9 is given by ✂(fMRI9)= $\{$—, $LIFG, (5, 1)\}$. In Appendix B, the background theories of Causal Scissor and CEC are addressed in more detail.

3 Experiment

3.1 Datasets

To validate the results of Causal Scissor, we experimented on five simulated data and three real-world data on biological and social science.

Synthetic dataset [18] provides a synthetic data that are generated by different dataset types according to four dimensions and two graph sampling schemes: *Erdős-Rényi* (ER) and scale-free (SF). In this experiment, following the nonlinear Gaussian ANM process, we set the number of nodes 10, the number of edges 40, the number of data samples 1,000, and *Erdős-Rényi* (ER) type.

fMRI9 dataset The dataset reselected from 9 individuals, originally collected from 13, is used to examine how the brain responds to temporal compression of speech and to determine whether the same regions such as Broca's and Wernicke's areas are engaged in phonological processes [24].

Sachs dataset This dataset is widely used for causal discovery about protein signaling pathways, consisting of 11 proteins using knockouts and spikings [25].

3.2 Model

[8] offers a sample-efficient score-based causal discovery via Bayesian optimization to recover an accurate DAG with minimal trials. Using DrBO (DAG recovery via Bayesian Optimization), causal graphs are generated and perturbations are done on the target variables. The perturbation is a hard intervention which directly sets a variable to a fixed value with the original dependencies removed. From the causal graphs of non-perturbation and perturbation, Ollivier-Ricci curvature, barycenter, and Gromov-Wasserstein distance are calculated. As a root cause discovery model, [19] shows a convincing method via permutations and Cholesky decomposition. Permutation invariance and Cholesky decomposition result in identifiability that may be non-identifiable under the causal ordering and the DAGs of n i.i.d. observational samples.

3.3 Results

Result of synthetic data (Synthetic data 0) As shown in Figure 9, the knock-on edges of Causal Scissor are $(5, 7)$ and $(6, 5)$ with the probability of CEC about 0.21 as in (f) of the figure. Plus, the root-cause nodes of Causal Scissor are $\{0, 2, 2, 9, 3, 3, 3, 3, 3, 3\}$ for each perturbation in consecutive order. Different from the naive facet that the number of cut edges in the graph under perturbation, as in (b), may be proportional to strongly perturbed subtrees, GW support indicates that perturbations 5 and 7 are above the mean of the total GW metrics like (c), representing the more negatively curved subtrees on manifold (as in the ν^+ of Figure 4). Causal Scissor of the synthetic data 0 is ✂(synthetic data 0)= $\{$—, $3, ((5, 7), (6, 5))\}$. To sum up the result of the synthetic data, principally the two knock-on edges and the root cause of node variable 3, the elements of Causal Scissor measured by CEC, are the causal by-product of $\texttt{do}(SyntheticData0)$.

Result of fMRI9 data In Figure 2, we have an interesting discovery that the causal variable, *LIFG*, is the top-GW root cause in Causal Scissor as in (c) of the figure. *LIFG* is left inferior frontal gyrus which is a critical brain region involved in various cognitive functions, particularly language processing and action. With a high CEC probability of about 0.24, the knock-on edge is $(5, 1)$ of the nodes *RACC* and *LACC* as in Figure 2. The Causal Scissor is, therefore, ✂(fMRI9)= $\{$—, $LIFG, (5, 1)\}$. This describes that a knock-on effect takes place on Barycenter Subtree 4 (blue causal flow) around the edge $(5, 1)$. With the Causal Scissor, note that perturbation 2 has the maximum of GW metrics.

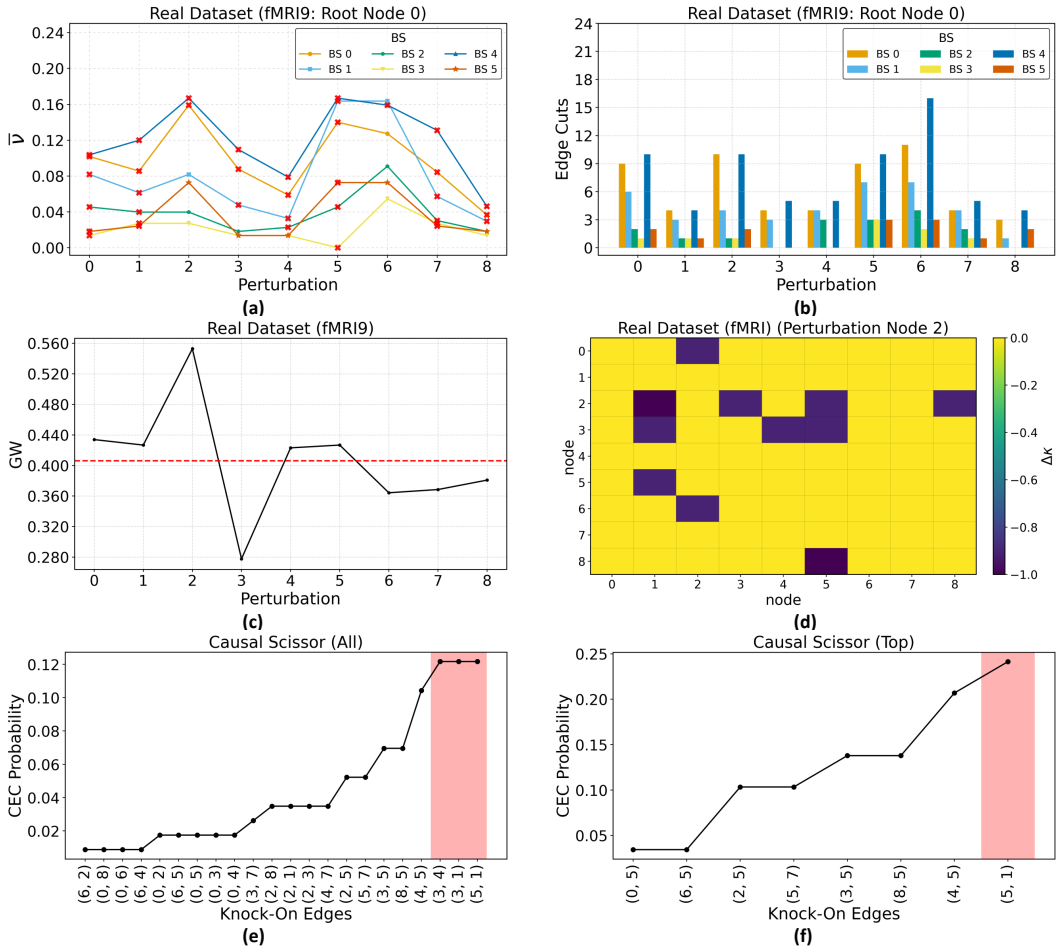

Figure 2: Causal Scissor result on the fMRI9 dataset: (a) Barycenter Subtrees per perturbation, (b) The number of BS-wise edge cuts per perturbation, (c) GW metric per perturbation with support baseline, (d) Heatmap of the difference of ORC $\Delta\kappa$, (e) CEC probability for knock-on edges above than GW, (f) Top-node's CEC probability of knock-on edges. The red markers, in (a), represent root causes in the subtrees.

Result of Sachs data Causal Scissor on Sachs data of a flow cytometry is ✂(Sachs)= $\{$—, $p44/42, (0, 1)\}$ as shown in Figure 7. p44/42 MAPK (Erk1/2) signaling pathway can be activated in response to a diverse range of extracellular stimuli, including mitogens, growth factors, and cytokines, which is considered as an important target in the treatment of cancer.

4 Conclusion

As a framework of subtree-wise causal discovery, we show that the causal structure under perturbation on manifold is relatively any of negatively curved simplex and CEC measures the perturbed curvature to discover the strongly perturbed knock-on edges and root causes via Barycenter subtree and GW support. Following that real-world causality is to be uncovered with the help of advanced causal representation learning, this interpretable mechanism on causal interdependency can serve to pinpoint the treatment or perturbation effects. Causal Scissor and CEC would be a step further toward the next glimpse in scientific causal discovery.

References

[1] Kartik Ahuja, Divyat Mahajan, Yixin Wang, and Yoshua Bengio. Interventional causal representation learning, 2022.

[2] Lorenzo Bini, Fatemeh Nassajian Mojarrad, Margarita Liarou, Thomas Matthes, and Stéphane Marchand-Maillet. Flowcyt: A comparative study of deep learning approaches for multi-class classification in flow cytometry benchmarking, 2024.

[3] Philippe Brouillard, Chandler Squires, Jonas Wahl, Konrad P. Kording, Karen Sachs, Alexandre Drouin, and Dhanya Sridhar. The landscape of causal discovery data: Grounding causal discovery in real-world applications, 2024.

[4] Zizhang Chen, Peizhao Li, Hongfu Liu, and Pengyu Hong. Characterizing the influence of graph elements, 2022.

[5] Davin Choo, Kirankumar Shiragur, and Caroline Uhler. Causal discovery under off-target interventions, 2024.

[6] Marco Cuturi and Arnaud Doucet. Fast computation of wasserstein barycenters. In Eric P. Xing and Tony Jebara, editors, *Proceedings of the 31st International Conference on Machine Learning*, volume 32 of *Proceedings of Machine Learning Research*, pages 685–693, Bejing, China, 22–24 Jun 2014. PMLR.

[7] Atray Dixit, Oren Parnas, Biyu Li, Jenny Chen, Charles P Fulco, Livnat Jerby-Arnon, Nemanja D Marjanovic, Danielle Dionne, Tyler Burks, Raktima Raychowdhury, Britt Adamson, Thomas M Norman, Eric S Lander, Jonathan S Weissman, Nir Friedman, and Aviv Regev. Perturb-Seq: Dissecting molecular circuits with scalable Single-Cell RNA profiling of pooled genetic screens. *Cell*, 167(7):1853–1866.e17, December 2016.

[8] Bao Duong, Sunil Gupta, and Thin Nguyen. Causal discovery via bayesian optimization, 2025.

[9] Amy Feng and Melanie Weber. Graph pooling via ricci flow, 2024.

[10] Lukas Fesser and Melanie Weber. Effective structural encodings via local curvature profiles, 2023.

[11] Lukas Fesser and Melanie Weber. Mitigating over-smoothing and over-squashing using augmentations of forman-ricci curvature, 2023.

[12] Lukas Fesser and Melanie Weber. Effective structural encodings via local curvature profiles, 2024.

[13] Bang-Xian Han, Deng-Yu Liu, and Zhuo-Nan Zhu. On the geometry of wasserstein barycenter i, 2024.

[14] Xiao Han, Lu Zhang, Yongkai Wu, and Shuhan Yuan. On root cause localization and anomaly mitigation through causal inference, 2022.

[15] Jaeseung Heo, Kyeongheung Yun, Seokwon Yoon, MoonJeong Park, Jungseul Ok, and Dongwoo Kim. Influence functions for edge edits in non-convex graph neural networks, 2025.

[16] Biwei Huang, Kun Zhang, Jiji Zhang, Joseph Ramsey, Ruben Sanchez-Romero, Clark Glymour, and Bernhard Schölkopf. Causal discovery from heterogeneous/nonstationary data with independent changes, 2019.

[17] Olivier Jeunen, Ciarán M. Gilligan-Lee, Rishabh Mehrotra, and Mounia Lalmas. Disentangling causal effects from sets of interventions in the presence of unobserved confounders, 2022.

[18] Sébastien Lachapelle, Philippe Brouillard, Tristan Deleu, and Simon Lacoste-Julien. Gradient-based neural dag learning, 2019.

[19] Jinzhou Li, Benjamin B. Chu, Ines F. Scheller, Julien Gagneur, and Marloes H. Maathuis. Root cause discovery via permutations and cholesky decomposition, 2024.

[20] Phillip Lippe, Sara Magliacane, Sindy Löwe, Yuki M. Asano, Taco Cohen, and Efstratios Gavves. Biscuit: Causal representation learning from binary interactions, 2023.

[21] Facundo Mémoli. Gromov–wasserstein distances and the metric approach to object matching. *Foundations of computational mathematics*, 11(4):417–487, 2011.

[22] Panagiotis Misiakos, Chris Wendler, and Markus Püschel. Learning dags from data with few root causes, 2023.

[23] Ricardo Pio Monti, Kun Zhang, and Aapo Hyvarinen. Causal discovery with general non-linear relationships using non-linear ica, 2019.

[24] Russell A. Poldrack, Elise Temple, Athanassios Protopapas, Srikantan Nagarajan, Paula Tallal, Michael Merzenich, and John D. E. Gabrieli. Relations between the neural bases of dynamic auditory processing and phonological processing: Evidence from fmri. *Journal of Cognitive Neuroscience*, 13(5):687–697, 07 2001.

[25] Karen Sachs, Omar Perez, Dana Pe'er, Douglas A. Lauffenburger, and Garry P. Nolan. Causal protein-signaling networks derived from multiparameter single-cell data. *Science*, 308(5721):523–529, 2005.

[26] Kirankumar Shiragur, Jiaqi Zhang, and Caroline Uhler. Meek separators and their applications in targeted causal discovery, 2023.

[27] Keanu Sisouk, Eloi Tanguy, Julie Delon, and Julien Tierny. Robust barycenters of persistence diagrams, 2025.

[28] Eric V. Strobl. Root causal inference from single cell rna sequencing with the negative binomial, 2023.

[29] Eric V Strobl and Eric R Gamazon. Discovering root causal genes with high throughput perturbations. February 2025.

[30] Eric V. Strobl and Thomas A. Lasko. Identifying patient-specific root causes of disease, 2022.

[31] Eric V. Strobl and Thomas A. Lasko. Sample-specific root causal inference with latent variables, 2022.

[32] Robert Tarjan. Depth-first search and linear graph algorithms. In *12th Annual Symposium on Switching and Automata Theory (swat 1971)*, pages 114–121, 1971.

[33] Jake Topping, Francesco Di Giovanni, Benjamin Paul Chamberlain, Xiaowen Dong, and Michael M. Bronstein. Understanding over-squashing and bottlenecks on graphs via curvature, 2021.

[34] Jake Topping, Francesco Di Giovanni, Benjamin Paul Chamberlain, Xiaowen Dong, and Michael M. Bronstein. Understanding over-squashing and bottlenecks on graphs via curvature, 2022.

[35] Petar Veličković. Everything is connected: Graph neural networks. *Current Opinion in Structural Biology*, 79:102538, April 2023.

[36] Dingling Yao, Caroline Muller, and Francesco Locatello. Marrying causal representation learning with dynamical systems for science, 2024.

[37] Çağlar Hızlı, ST John, Anne Juuti, Tuure Saarinen, Kirsi Pietiläinen, and Pekka Marttinen. Causal modeling of policy interventions from sequences of treatments and outcomes, 2022.

A Appendix

We categorize edge states in conjunction with perturbation or intervention into four types, of which combination constitutes the building block of perturbed causal structures.

- Type 1 (**Edge cutting**): Interventions yield the causal graphs to be cut that a causal variable A does not affect a causal variable B any more, as an extrinsic edge change.
- Type 2 (**Edge mutant**): Interventions have different effects without cutting that a causal variable A affects a causal variable B maintaining the causal connectivity, as an intrinsic state change.
- Type 3 (**Edge inversion**): As a result of interventions, the change of causal direction appears that the prior edge from A to B are inverted into B to A after perturbation.
- Type 4 (**Edge reassembly**): Besides the types 1 to 3, the edges would be reassembled to other nodes that the posterior causal states are different from the prior.

In the above perturbed edge types, this work deals with the edge cutting (Type 1).

B Preliminaries

As a causal flow framework, we set three mapping spaces: observational, underlying causal, and geometric spaces; each variable as x_i, z_j, κ_k and $i \in \mathbb{R}^d$, $j \in \mathbb{R}^{d\times d}$, $k \in M$ where each is in the form of scalar, matrix, and curvature respectively. Without loss of generality, variables in the paper are represented on manifold. First, existing directed acyclic graph (DAG) models are employed for causal graphs. More concretely, from given biological data causal graphs or DAGs are generated by a Bayesian optimization model (e.g. DrBO), then the graphs are converted into manifold space for measuring the effects of intervention. Our goal is to represent the mechanism of perturbational causal flow in the graphs by using CEC that measures the influence of removed or cut edges through subtree-wise causal flows via optimal transport.

Our primary interest to tackle the two questions in Introduction starts from an assumption that perturbation may cause the change in the number of connected edges on a causal graph with a structural pattern. Motivated by [33] that the bottleneck on a graph via curvature gives a clue to understand the oversquashing problem for the interaction of distant nodes, we focus on the interaction of cut edges with root causes via curvature.

Considering the existing studies on the perturbed change for edges, edge edits mean to insert or remove edges in a causal graph for node prediction and classification [15]. Edge removal would incur a knock-on effect to break down all message passing on a graph [4]. [22] proposes a DAG learning with few root causes while root causes and their influenced edges on a manifold can provide more interpretable scientific discovery such as on Sachs dataset because underlying causal factors are entangled in dependency, whereas curvature reveals the flows in a schematic manner like a transport map to find the best coupling.

Definition B.1 (Root cause)**.** Given a perturbed variable $x \in \hat{\mathcal{X}}^-$, the root cause of x is a set of graph features that response to the perturbation leading to a significant change in the post graph distribution, e.g. knock-on edges [14].

Definition B.2 (knock-on edges)**.** Root causes yield knock-on effects so that the child edges would cut or removed by the impact on the perturbation and root causes. Those cut edges are termed as knock-on edges which are an element of Causal Scissor, measured by CEC with local Ollivier-Ricci curvature and subtree-wise barycenter.

B.1 Causal Scissor

Seeing through the lens of curvature structural encoding, root causes and knock-on edges which belong to Causal Scissor are able to be unlocked with expressive power to explain the inherent mechanism of causal variables. Causal Scissor represents strongly perturbed subtrees having knock-on edges and root causes. CEC, the mixture of Wasserstein metrics, provides the measure to discover Causal Scissor.

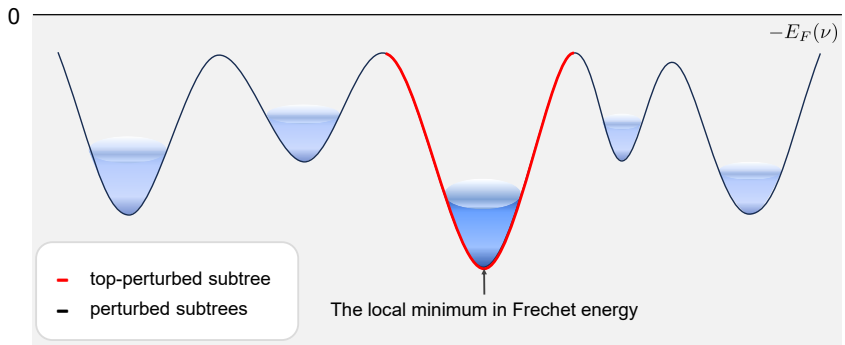

Figure 3: A subtree barycenter located at the local minimum of the Fréchet energy belongs to top-perturbed subtree.

Let a causal graph be $G = (V, E)$, a set of nodes V and neighboring edges $(u, v) \in E$. We denote the adjacency matrix by A. $\mu_i(z) = \frac{1}{\deg(i)}$ is the uniform marginal measure where z is a neighbor of $i \in \{u, v\}$. We adopt Ollivier-Ricci curvature, which calculates the edge-wise distributional difference of the adjacency matrix in a given causal graph.

For nodes $i,\ j \in V$ and their probability distributions μ_i, μ_j, the optimal transport distance can be computed as in [9]

$$W_1(\mu_i, \mu_j) = \inf_{\mu \in \Gamma(\mu_i, \mu_j)} \int d_{\mathcal{M}}(x, y)\mu(x, y)dxdy,$$

where $d_{\mathcal{M}}(x, y)$ represents the geodesic distance, and $\Gamma(\mu_i, \mu_j)$ the set of measures with marginals μ_i, μ_j. From the Wasserstein-1 distance, the Ollivier-Ricci Curvature is given by $\kappa_{\mathcal{M}}(x, y) = 1 - \frac{W_1(\mu_x^{\mathcal{M}}, \mu_y^{\mathcal{M}})}{d_{\mathcal{M}}(x,y)}$.

CEC measures $p(\texttt{cut}(\cdot))$, the probability of strongly influenced cut edges, via ORC given how much the perturbation or $\texttt{do}(\cdot)$ flows to the edges. To facilitate the causal flow toward intervened child nodes or root causes, we classify the causal graphs into subtrees by using depth-first search [32]. Based on the subtrees, we compute barycenters averaged in Wasserstein-2 distance where Causal Scissor, the set of ν^+ subtrees, belongs to the local minima of the Fréchet energy [6] (Refer to Figure 4).

Throughout this paper, ✂ denotes Causal Scissor which is a set of strongly perturbed subtree with the elements of a root cause and knock-on edges, defined as follows.

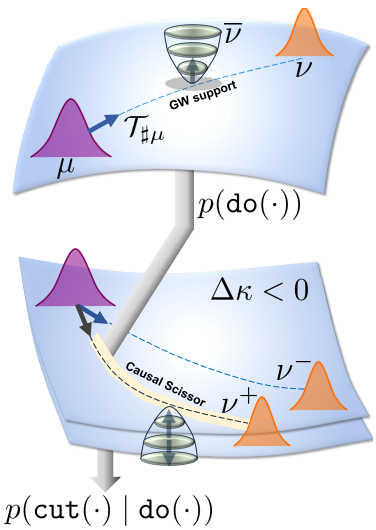

Figure 4: (top) A non-perturbed curvature, (down) A perturbed curvature. Strongly perturbed subtrees are located in the causal flows on a relatively more negative curvature. In the lower part of the figure, the barycenter ν^+ with Causal Scissor can take a larger support than ν^- with a weak causal flow where the barycenter bowl represents the level of support as the upward and downward arrows. A Causal Scissor flows along on a negative curvature with a larger barycenter and GW support.

Definition B.3 (Causal Scissor)**.** Causal Scissor is a tuple-like set of three elements on a given data such that

✂(data)=
$\{$(*BS, RC, KOE*) | *BS* is the most strongly perturbed subtree, *RC* root causes, and *KOE* knock-on edges$\}$.

From the following theorems, Causal Scissor is of the strongly barycentrically convex on local and global curvature, and in the local minima in Fréchet energy.

On root cause, barycenter and Gromov-Wasserstein support

[19] suggests that the combination of permutation and the Cholesky decomposition leads to search for an invariant property related to the root causes. We regard the root causes as the local minima in Fréchet energy measured by barycenter in that the most strong knock-on edges are located near the subtrees of root causes. As the barycenters of subtrees encode the salient features in data, we measure the subtree-wise barycenters by perturbation on biological data to show that root causes correspond to the largest values of barycenters.

Assume that μ_α is a causal edge mass, the amount of mass moved with distance α in optimal transport. In case of $\alpha \leq 3$, the Ollivier-Ricci curvature is expressed as a causal edge mass by $\kappa = \mu_0 - \mu_2 - \mu_3$. Optimal transport generally finds the best coupling between two distributions, which leads to the barycenter that is a metric averaging in Wasserstein distance. The barycenters per subtree are the centroid of perturbed graphs; the larger the barycenter, the more curved the manifold, and the stronger the perturbation.

Theorem 1. *The strongly influenced flow is more curved than the weakly influenced flow.*

Proof. Let $d_{\mathcal{M}}(x, y) = 1$ in a causal graph. Since the mass of strongly influenced edges μ_α^+ is relatively equal or small in that they are less optimal-transport by causal cuts compared to the mass of weakly influenced edges μ_α^- with the same μ_0, in case of $\alpha \leq 3$, the curvature difference of strongly and weakly influenced edges is

$$\begin{aligned} \kappa^+ - \kappa^- &= (\mu_0 - \mu_2^+ - \mu_3^+) - (\mu_0 - \mu_2^- - \mu_3^-) \\ &= (\mu_2^- - \mu_2^+) + (\mu_3^- - \mu_3^+) \\ &\geq 0. \end{aligned} \tag{3}$$

□

Theorem 2. *Let a root-cause node u_{rc}, a non- or weakly perturbed edge $e^-(u, v)$ and a knock-on or strongly influenced edge $e^+(u, v)$. Accordingly the subtree with high barycenter has more e^+ than the one with low barycenter. Assuming that W_1 in ORC and W_2 in barycenter have similar tendencies, the inequality for weakly perturbed and strongly perturbed barycenters per subtree in terms of curvature is hold*

$$\overline{\nu}^-(\kappa) \leq \overline{\nu}^+(\kappa)$$

as the curvature of non- or weakly perturbed edges is less than or equal to the curvature of strongly perturbed ones from their edge marginals μ_i.

Proof. Since the barycenter $\overline{\nu}$ is argmin of W_2^2 from Eq. 2, and $\kappa^+ \geq \kappa^-$ from Eq. 3, and $\kappa \approx 1 - W$, thus $\overline{\nu}^+ \geq \overline{\nu}^-$. □

In other words, root causes have more strongly influenced (knock-on) edges around their neighbors. The criteria between weakly and strongly influenced edges are based on GW distance. We set the criteria according to the mean value of GW distance for the causal structure whether a given subtree belongs to weakly influenced edges or a strongly influenced edges. The criteria via GW distance are treated as support, a value that each latent can possibly take. For example, when two latents z_1, z_2, a parent and a child, that have no dependency or are in the state with causal cuts are independent support [1].

GW support Gromov-Wasserstein (GW) support is a global-hyperbolicity support on measure space $(\mathbb{R}^d,\ \mathcal{B},\ \overline{\nu})$, i.e. what values each latent can possibly take and the set where the probability density is non-zero such that for a random variable X, the support $\mathcal{X} = \left\{x \in \mathbb{R}^d, d\mathbb{P}_X > 0\right\}$ where $d\mathbb{P}_X$ is the Radon-Nikodym derivative of $\mathbb{P}$ with respect to barycenter measure over completion of Borel sets on $\mathbb{R}^d$. For a random variable Z, $\mathcal{Z}$ is the support of Z in the observational data and $\mathcal{Z}^{(i)}$ is the support of Z when Z_i, a component of Z, is perturbed.

Theorem 3. *There exists a lower bound of mean barycenter to determine a support.*

Proof. Let $(X,\ d)$ be a barycenter space. Given $K \in \mathbb{R}$, a function $F : X \to \mathbb{R} \cup \{+\infty\}$ is called to be weakly or strongly K-barycentrically convex if for any $\mu \in \mathcal{P}(X)$ with finite variance, there is a barycenter $\overline{x}$ of μ, as in [13], such that

$$F(\overline{x}) \leq \int F(x)d\mu(x) - \frac{K}{2}Var(\mu). \tag{4}$$

By the Jensen's inequality of Wasserstein barycenter and $Var(\mu) = E(\mu^2) - \overline{\mu}^2$, Eq. 4 is

$$F(\overline{x}) \leq \int F(x)d\mu(x) - \frac{K}{2}\left[E(\mu^2) - \overline{\mu}^2\right].$$

Therefore,

$$E(\mu^2) + \frac{2}{K}\left[F(\overline{x}) - \int F(x)d\mu(x)\right] \leq \overline{\mu}^2,$$

where the square root of the left-hand side is a lower bound of the mean barycenter.

□

On relatively negative curvature Let $\Delta\kappa$ be the difference of non-perturbed and perturbed curvatures, i.e. $\kappa_{\texttt{non}} - \kappa_{\texttt{do}}$. A transport map from a parent node μ to its child node ν is $\mathcal{T} : \mathbb{R}^d \to \mathbb{R}^d$ from μ to ν. We assume that two causal flows, for example, may take totally different transport maps between μ and ν since optimal transport or Wasserstein metric explores to find the best coupling or flow $\mathcal{T}^*$ where the curvature of the causal walks or flows obviously differ as in Figure 4; in case of a strong perturbation, $\Delta\kappa$ tends to be negative as shown in (d) of Figure 2, likewise the gap curvatures of other data.

B.2 Related works

Causal discovery for science Causal discovery for climate change would be a demanding challenge for real-world solutions. [36] provides a causal representation learning to dynamical systems by applying the model to real-world climate change data. Causal discovery under intervention is another significant problem to tackle in various scientific fields. [26] focuses on the targeted causal discovery to learn causal structures from interventional data under the scenarios that only part of the causal graph is available. In addition, [5] proposes a stochastic intervention model to minimize the number of intervention. Particularly [16, 23] propose the methods of causal discovery on fMRI where the latter infers non-linear relationships between passively observed variables with an alternative measure of causal direction.

Root causes In biological research, identifying root causes would have momentum because of the availability of perturbation data and causal representation learning [31, 28, 19]. For example, Perturb-seq, high throughput 13 perturbations with single cell RNA-seq readout, is used to learn the causal order between the genes, and the Heteroscedastic Noise Model on PBC (Mayo Clinic Primary Biliary Cholagitis) and Framingham Heart Study (FHS) dataset is able to identify patient-specific root causes [30, 29].

Curvature and barycenter Rewiring has been attracted increasing attention because of its ability to improve the performance of graph neural networks by mitigating oversmoothing and oversquashing [12]. As a way to rewiring to distant nodes, curvature captures structural information over a node's two-hop neighborhood, in contrast to the one-hop ways of general message passing.

To address the graph bottleneck and alleviate the oversquashing, [34] proposes Stochastic Discrete Ricci Flow in that the negatively curved edges cause the oversquashing problem. This problem, on the contrary, gives us a hint that non-perturbed and perturbed curvatures, on a relative manifold, may be negatively curved or have bottlenecks around knock-on edges due to perturbation. Consequently strongly negatively curved edges under perturbation cause the overcutting problem as we propose in this literature.

C Additional results

C.1 Sachs dataset

Sachs dataset is the general benchmark dataset for the causal discovery of protein signaling networks which is based on multiparameter single-cell flow cytometry. The dataset is designed to explore well-known pathways such as Raf–MEK–ERK cascade, PI3K–Akt pathway, and PKC signaling, and is specialized for the single-cell measurement of thousands of human $CD4^+ \ T_h$ cells. In this paper, we experimented on 11 variables and 853 samples.

When it comes to the causal flows of Sachs data, as shown in (b) of Figure 6, under perturbation to node 5 (*p44/42* or ERK), the edge between *praf* and *pmek* is knocked on. *praf* is a variable of Raf phosphorylation of which signal is connected to the parent nodes of Raf–MEK–ERK paths. *pmek* is a variable of Ser217/Ser221 phosphorylation for MEK1/2.

C.2 Teacher Burnout dataset

This dataset in social science is primarily intended to investigate the importance of particular background variables on three factors of burnout (emotional exhaustion, depersonalization, reduced personal accomplishment) for elementary, intermediate, secondary, and university teachers. Based on the repository of [3], perturbations are done on 9 items (RA1, RA2, RC1, RC2, WO1, WO2, CC1, CC2, CC3) out of 32 items to measure CEC and discover Causal Scissor.

As shown in Figure 8, Causal Scissor is ✂(TeacherBurnout)= $\{$—, $RA2, ((5, 24), (5, 25), (27, 5))\}$. Also the knock-on edges, with CEC probability 0.33, are (5, 24), (5, 25), and (27, 5) where node 5 is *WO2*. *RA2* (role ambiguity 2) is the root cause that has knock-on edges like (c) of Figure 6. It means that *DP1* (depersonalization 1) strongly causes *WO2* (work overload 2) which then affects *EE1, EE2* (emotional exhaustion), all initiated from *RA2* (role ambiguity 2).

C.3 Synthetic data 1

As a result of synthetic data 1, the root causes are $\{4, 1, 4, 4, 1, 1, 6, 1, 4, 9\}$ for each perturbation. Like Figure 10, Causal Scissor is ✂(synthetic data 1))= $\{$—, $(1, 4), ((3, 4))\}$ with CEC probability 0.23.

C.4 Synthetic data 2

As a result of synthetic data 2, the root causes are $\{4, 1, 0, 5, 4, 4, 5, 5, 8, 0\}$ for each perturbation. Like Figure 11, Causal Scissor is ✂(synthetic data 2)= $\{$—, $5, ((3, 4), (3, 5), (3, 8))\}$ with CEC probability 0.33.

C.5 Synthetic data 3

As a result of synthetic data 3, the root causes are $\{2, 2, 5, 2, 8, 5, 6, 2, 4, 9\}$ for each perturbation. Like Figure 12, Causal Scissor is ✂(synthetic data 3)= $\{$—, $2, ((0, 1), (0, 7))\}$ with CEC probability 0.23.

C.6 Synthetic data 4

As a result of synthetic data 4, the root causes are $\{7, 7, 7, 7, 4, 7, 6, 3, 6, 7\}$ for each perturbation. Like Figure 13, Causal Scissor is ✂(synthetic data 4)= $\{$—, $7, ((7, 2), (7, 3), (7, 9))\}$ with CEC probability about 0.18.

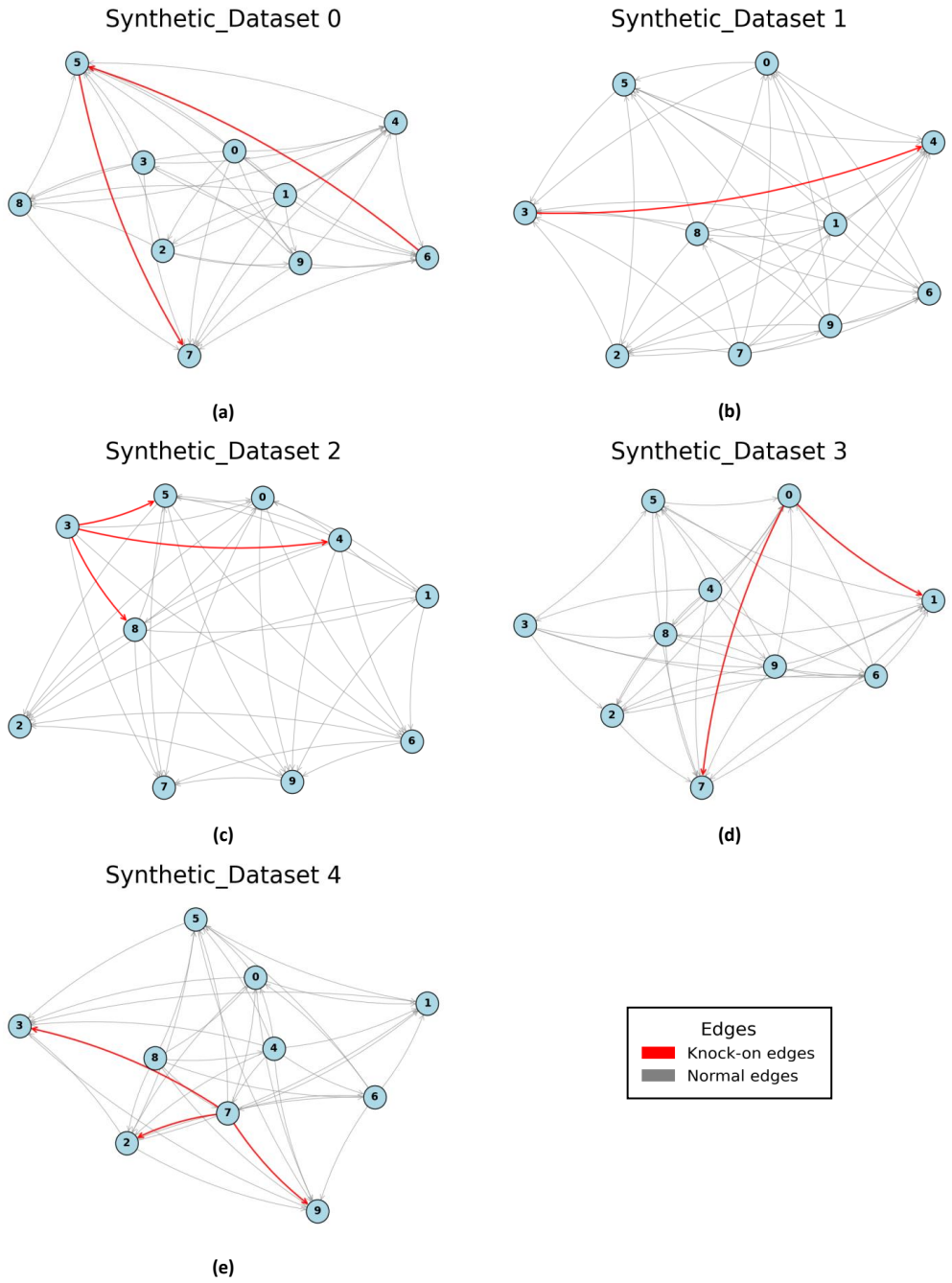

Figure 5: Causal graphs on experiment synthetic datasets. The red edges represent knock-on edges.

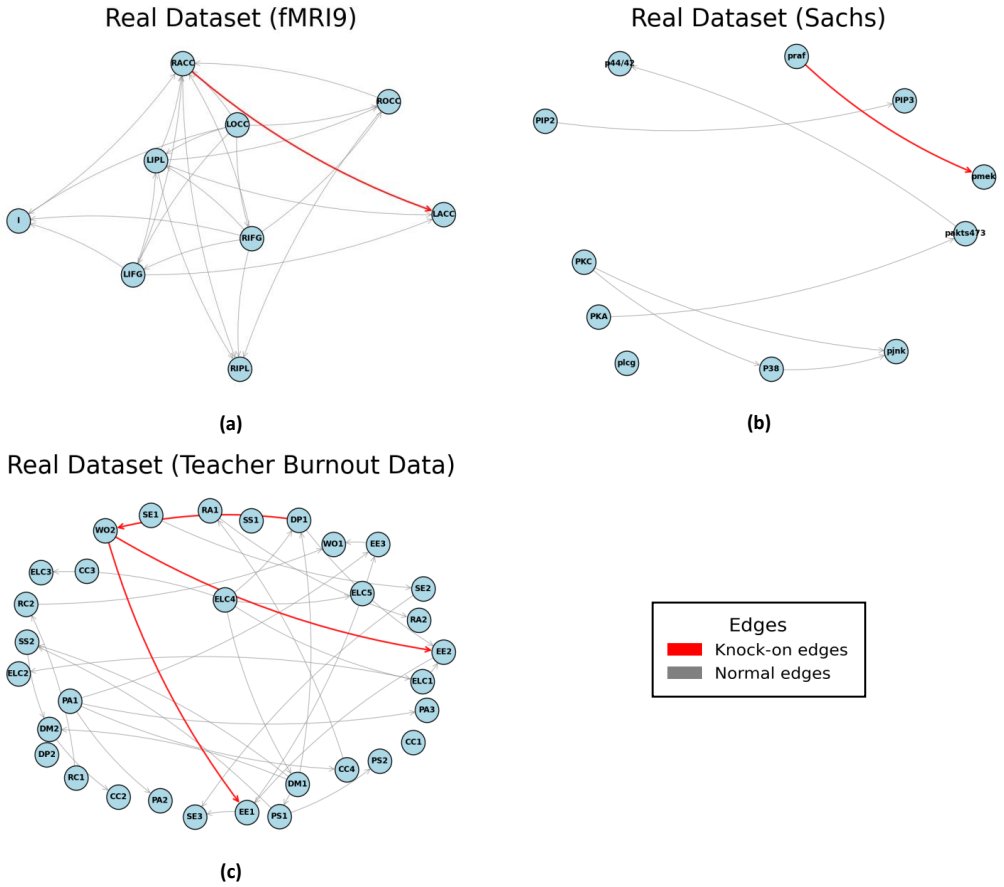

Figure 6: Causal graphs on experiment real datasets. The red edges represent knock-on edges.

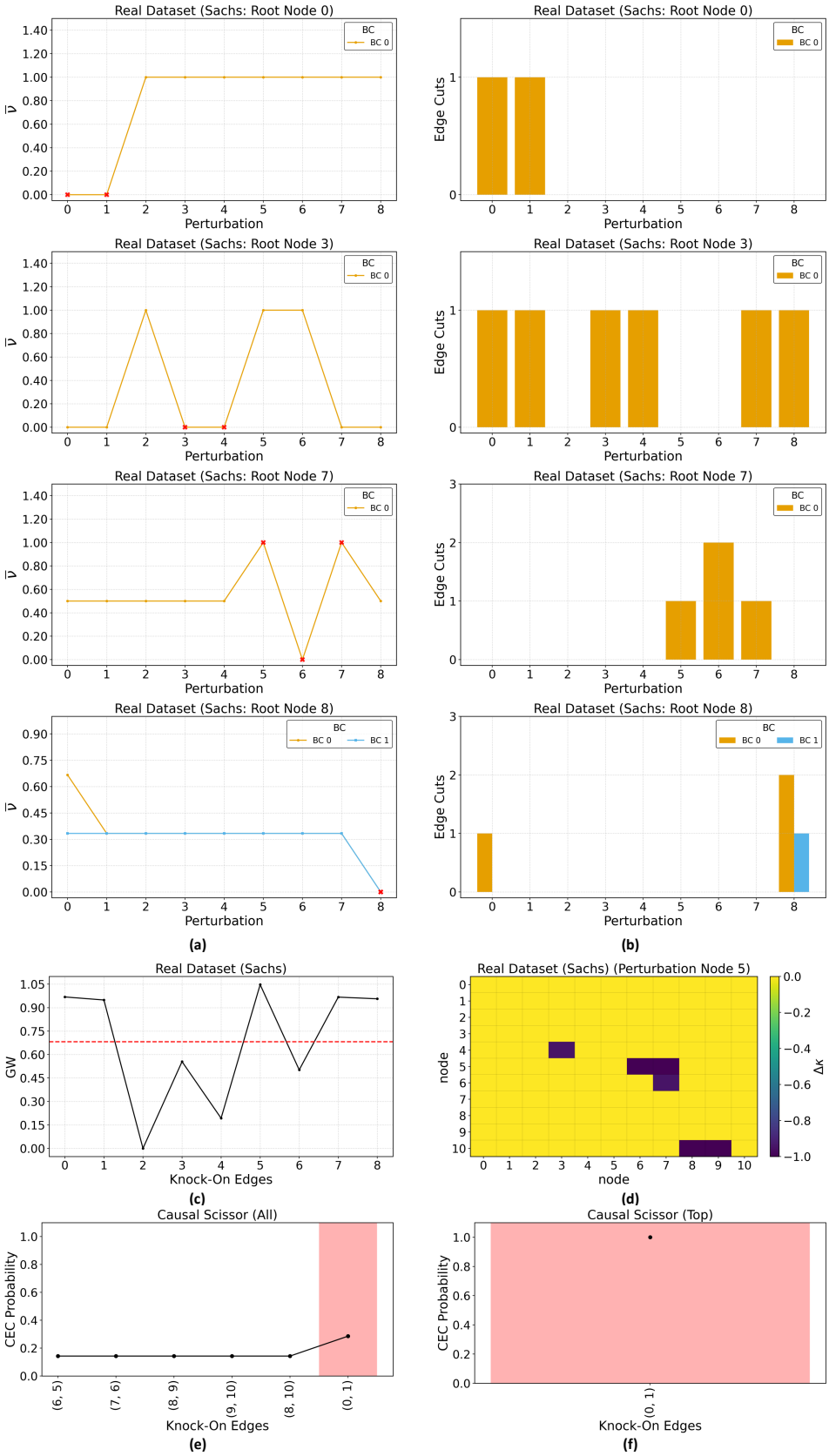

Figure 7: Causal Scissor result on Sachs dataset

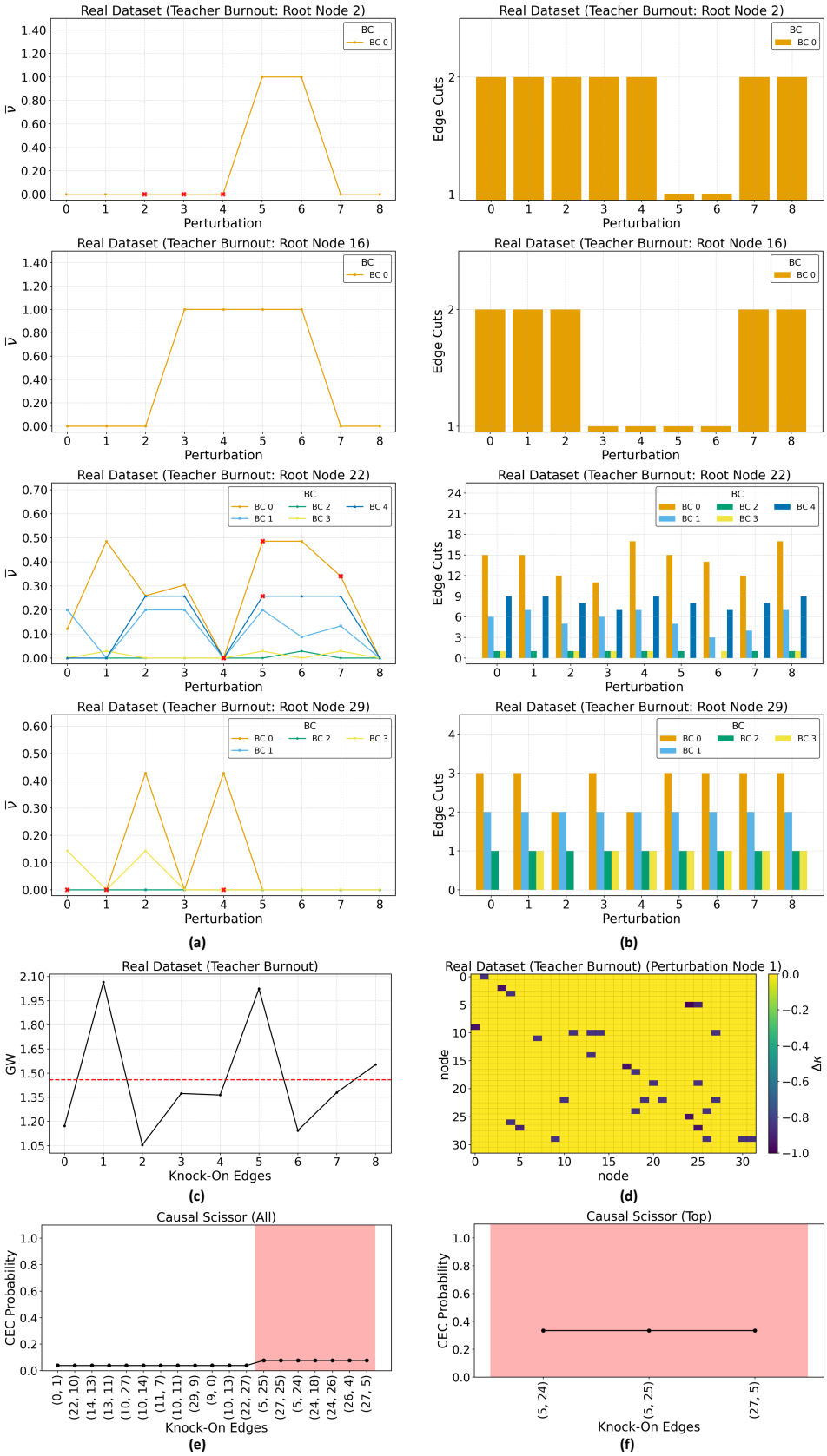

Figure 8: Causal Scissor result on Teacher Burnout dataset

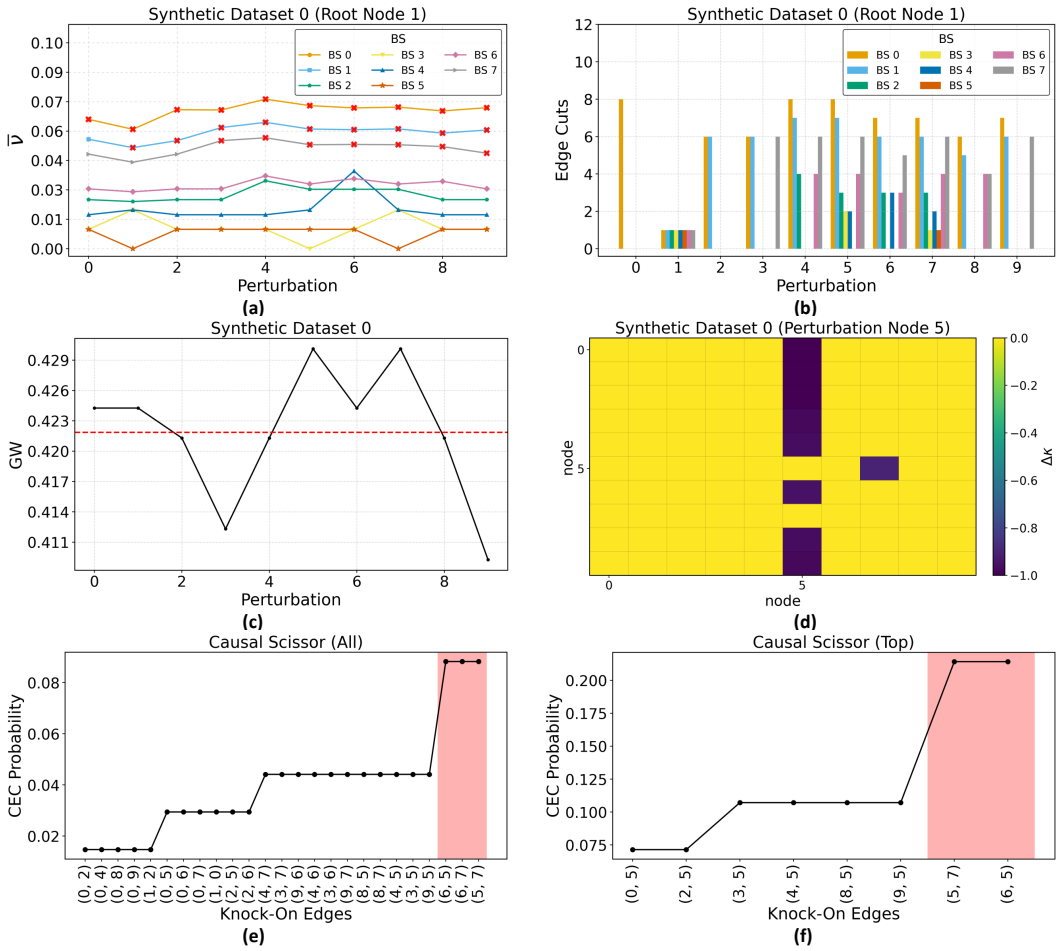

Figure 9: Causal Scissor result on the synthetic dataset 0

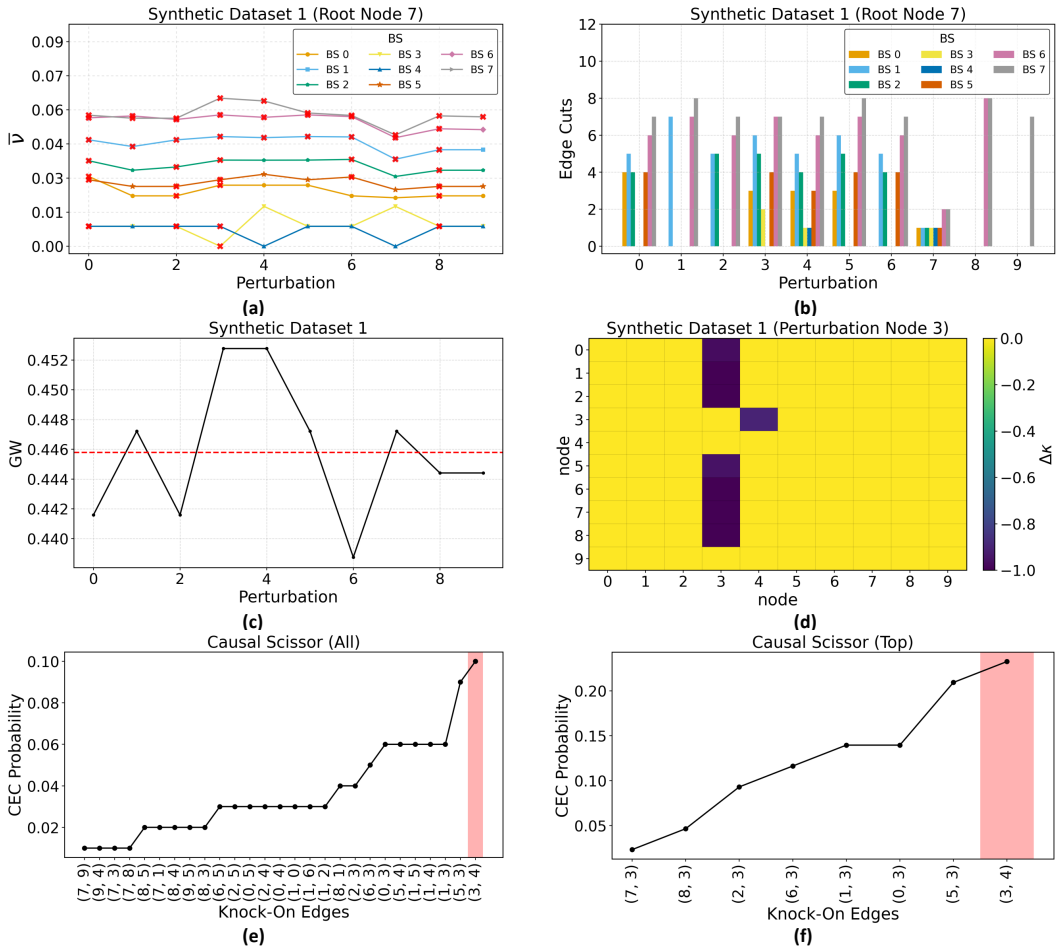

Figure 10: Causal Scissor result on the synthetic dataset 1

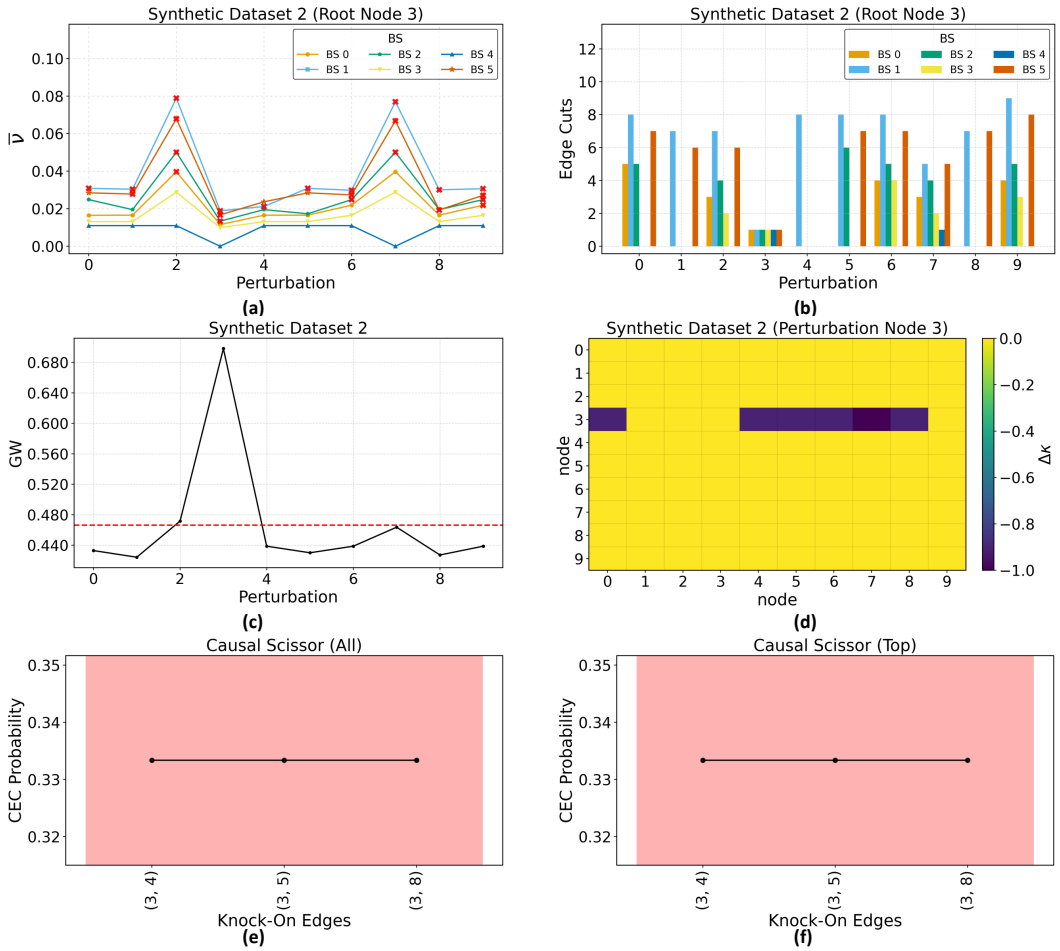

Figure 11: Causal Scissor result on the synthetic dataset 2

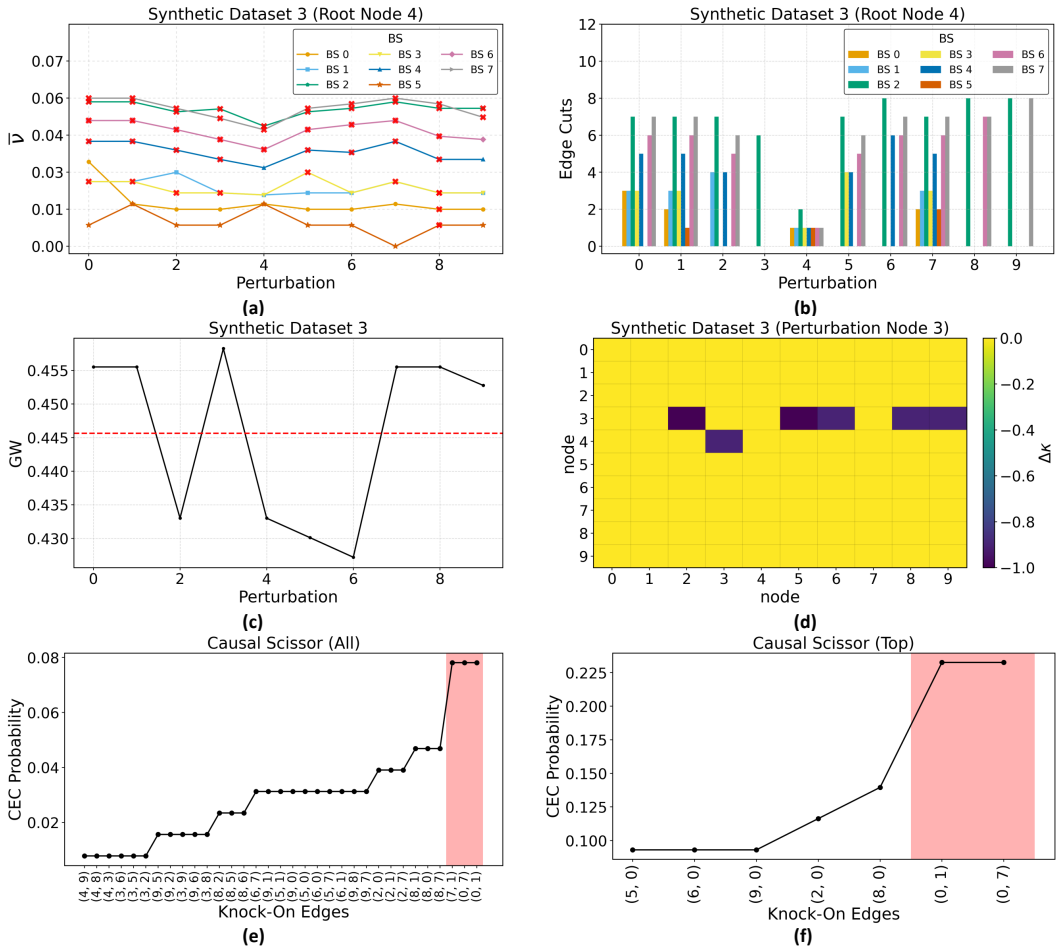

Figure 12: Causal Scissor result on the synthetic dataset 3

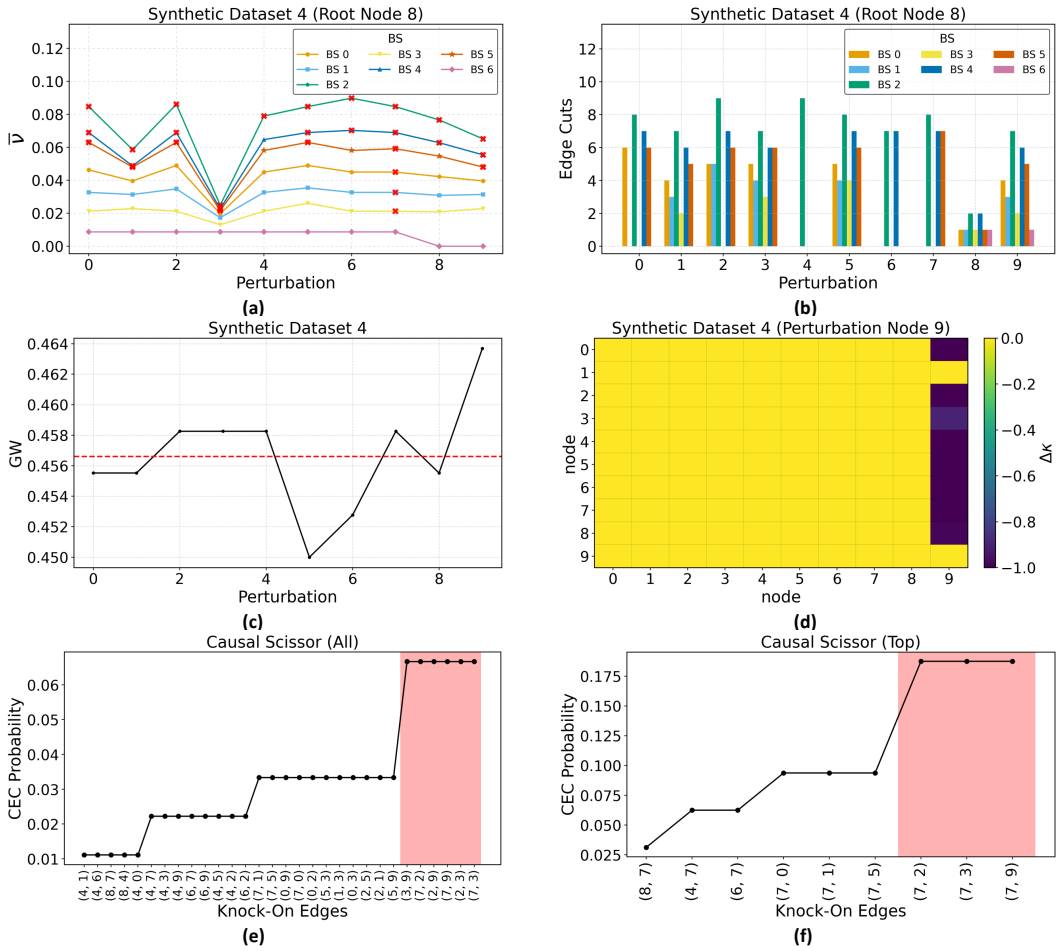

Figure 13: Causal Scissor result on the synthetic dataset 4